



1

1 **Coastal and regional marine heatwaves and cold-spells in**
2 **the Northeast Atlantic**

3

4

5

6

7

8

9

10

11

12

13

14

15

16

17

18

19

20

21

22

23

24

25

26

27

28

29

30

31

32

33

34

35

36

37

38

39

40

41

42

43

44

45

46

47

48

49

Amélie Simon^{1*}, Coline Poppeschi² Sandra Plecha¹,
Guillaume Charria², Ana Russo¹

¹ Universidade de Lisboa, Faculdade de Ciências, Instituto Dom Luiz (IDL), 1749-016, Lisboa, Portugal

² Ifremer, Univ. Brest, CNRS, IRD, Laboratory for Ocean Physics and Satellite remote sensing (LOPS), IUEM,
29280 Brest, France

*corresponding author: Dr. Amélie Simon; ajsimon@fc.ul.pt

Abstract

The latest IPCC report describes an increase in the number and intensity of marine heatwaves (MHWs) and a decrease in marine cold-spells (MCSs) in the global ocean. However, these reported changes are not uniform on a regional to local basis and it remains unknown if coastal areas follow the open ocean trends. Ocean temperature measurements collected by satellites (from 1982-2022) and 13 coastal buoys (from 1990-2022) are analyzed in the Northeast Atlantic and three subregions: English Channel, Bay of Brest and Bay of Biscay. The activity metric, combining the number of events, intensity, duration and spatial extent, is used to evaluate the magnitude of these extreme events. The results from *in situ* and satellite datasets for each of the studied regions are quite in agreement, although the satellite dataset underestimates the amplitude of activity for both MHW and MCS. This supports the applicability of the method to both *in situ* and satellite data, albeit with caution on the amplitude of these events. Also, this localized study in European coastal Northeast Atlantic water highlights that similar changes are being seen in coastal and open oceans regarding extreme events of temperature, with MHWs being more frequent, longer, and extending over larger areas, while the opposite is seen for MCSs. These trends are explained by changes in both the mean and variance of sea-surface temperature. Besides, the pace of evolution and dynamics of marine extreme events differs among the subregions. The English Channel is the region experiencing the most drastic changes over the last four decades. Summer marine heatwaves were very active in the English Channel in 2022 due to long events, in the Bay of Biscay in 2018 due to intense events and in the Bay of Brest in 2017 due to a high occurrence of events. Winter MCSs were the largest in 1987 and 1986 due to long and intense events in the English Channel. Finally, our findings suggest that at an interannual time scale, having dominant high-pressure conditions over Northern Europe and a low off the Iberian Peninsula favor the generation of strong summer MHWs in the Northeast Atlantic, while the opposite situation in winter dominates for MCSs.



2

50 2

51

52

53

54 **Summary**

55 In the coastal Northeast Atlantic and for three subregions (the English Channel, Bay of Brest
56 and Bay of Biscay) over the period 1982-2022, marine heatwaves are more frequent, longer,
57 and extending over larger areas, while the opposite is seen for marine cold-spells. This result
58 is obtained with both in-situ and satellite datasets, although the satellite dataset underestimates
59 the amplitude of these extreme events.

60

61 **Keywords**

62

63 Extreme events, Sea Surface Temperature, Long-term *in situ* observations, Satellite data,
64 Marine heatwaves, Marine cold-spells, Bay of Biscay, English Channel, North Atlantic
65 Oscillation

66

67

68

69

70 **1. Introduction**

71

72 Heatwaves and cold-spells are extreme events in which there is a significant difference
73 in temperature for a certain period, more or less extensive, and which can persist for several
74 months in vast areas of the planet (Hobday et al., 2016). This type of phenomenon can occur
75 both in the atmosphere and in the ocean, with remarkable consequences both for terrestrial
76 and marine ecosystems (Ruthrof et al., 2018). In the case of marine events (hereafter referred
77 to as marine heatwaves (MHWs) or marine cold-spells (MCSs)), severe large-scale
78 biodiversity losses may occur such as species extinction, habitat destruction and abrupt
79 changes in the geographical distribution and structure of communities, as well as the nutrient
80 cycle (Frölicher and Laufkötter, 2018; Ruthrof et al., 2018; Smale et al., 2019). Additionally,
81 a decrease in the density of marine algae forests and coral bleaching (Wernberg et al., 2016;
82 Smale et al., 2019) have also been reported.

83 The frequency, duration and intensity of these extreme phenomena affecting ocean
84 systems have been increasing worryingly in recent decades (Oliver et al., 2018; Frölicher et al.,
85 2018; Plecha and Soares, 2020; Simon et al., 2022 and many others). As a result of global and
86 regional warming heavily influenced by anthropogenic factors, the intensity and annual
87 number of MHW will continue to accelerate globally (Oliver et al., 2019; Plecha et al., 2021).
88 Conversely, as oceans warm, MCSs are diminishing (Schlegel et al., 2021; Simon et al., 2022)
89 and are expected to continue fading in future climate conditions (Yao et al., 2022). However,
90 these evolutions are not uniform regionally and it remains unknown if coastal areas follow the
91 open-ocean trends.

92 Long-term ocean warming is an important driver of the increase of MHW (Frölicher et
93 al., 2018) and the diminishing of MCS (Schlegel et al., 2021; Wang et al., 2022) but does not
94 explain shorter variabilities of these events, or justify their interannual variability. These



95 marine extreme events are also driven by other local and remote processes acting across a
96 large range of spatial and temporal scales (Holbrook et al., 2019; Schlegel et al., 2021).
97 Modes of atmospheric circulation variability can induce anomalous sea surface temperatures
98 (SST) through modification of air-sea heat fluxes and/or displacement due to ocean current
99 advection (Deser et al., 2010) which for extreme cases, can lead to MHW or MCS.

100 Interannual summer atmospheric variability in the North Atlantic-European sector has
101 been shown to be predominantly led by the summer North Atlantic Oscillation (SNAO)
102 pattern. The SNAO is identified as strong high-pressure anomalies dominating Northern
103 Europe and weaker low-pressure over Greenland and the Iberian Peninsula which explains
104 about 20% of the variance using sea-level pressure (Hurrell et al., 2003). The SNAO is
105 recognized as a more northerly location and smaller spatial scale than the winter NAO pattern.
106 During the positive phase of the SNAO, Northern Europe experiences drier, warmer and
107 reduced cloudiness conditions, and the Bay of Biscay, the English Channel, and the North and
108 Baltic Seas undergo warmer SST (Folland et al., 2009). The East Atlantic (EA) pattern is also
109 identified as a dominant mode of North Atlantic atmospheric variability (Barnston and
110 Livezey, 1987), which is particularly important for the northwest Iberian Peninsula climate in
111 all seasons (Lorenzo et al., 2008). It is a North–South dipole that spans the entire North
112 Atlantic Ocean, with centers southeastward to the NAO pattern (winter and summer).

113 Although there is strong evidence of the influence of large-scale features, no
114 consensus exists on atmospheric patterns associated with summer MHW in the Bay of Biscay
115 and the English Channel. On one side, Holbrook et al. (2019) identify the Bay of Biscay as a
116 region for which there is a significant increase in MHW days during a positive phase of the
117 NAO, based on a linearly detrended SST with satellite data and NAO index. On the other
118 side, Izquierdo et al. (2022a) suggest, based on the analysis of two *in situ* buoys in the coastal
119 south of the Bay of Biscay, that the incidence, duration, and intensity of MHW is higher
120 during the positive phase of the EA. However, for each of these two studies, only one climate
121 index out of the numerous modes of summer atmospheric variability in the North Atlantic-
122 Europe sector was considered. MCSs have also been reported to occur as a response to
123 atmospheric forcing through anomalous winds and air-sea heat fluxes, especially in coastal
124 regions where cold air outbreaks over shallow water can cause rapid chilling of water (Crisp,
125 1964; Schlegel et al., 2021). But to the best of our knowledge, no study has been published
126 focusing on the connection between MCS and atmospheric circulation in the Bay of Biscay
127 and the English Channel.

128
129 At a more regional scale, Guinaldo et al. (2022) linked the 2022 MHW off France to
130 solar radiation, cloud coverage and wind anomalies showing also the importance of
131 hydrodynamic conditions such as the tide that allows turbulent vertical mixing. This explains
132 why the Mediterranean sea with weak tidal ranges presents a more pronounced response to
133 MHW (Darmaraki et al., 2019; Simon et al., 2022). Other studies have been carried out in
134 terms of processes and detection of MHW in the Bay of Biscay but only along the Spanish
135 Cantabrian coast. Namely, Izquierdo et al. (2022b), found a steady increase in SST from 1998
136 to 2019, which was reflected in MHW occurrence and consequent match-up to report
137 population shifts in coastal macroalgae. In a second study, Izquierdo et al. (2022a) compared
138 MHW with satellite data and found a 6-fold increase in their incidences in the last 4 decades
139 with half of this increase related to climate change.

140 Several studies focus on the impact of MHW or MCS on biological systems, covering
141 the areas of the Bay of Biscay, the English Channel or the Spanish Cantabrian coast, reaching
142 as far back as the 60s of the XXth century. These studies analyzed the atmospheric cold-spells
143 of the winter of 1962-1963 on the English coast and the impact on marine animal mortality
144 such as *Pecten Maximus* (Crisp, 1964) or migration of species such as flounder (Sims et al.,



4

145 2004). In the English Channel, Gomez and Souissi (2008) made the link between the MCS of
146 2005 and the absence of the spring bloom of *Phaeocystis*. A delay in the initiation of the
147 phytoplankton bloom caused by the presence of MCS at the end of winter in the Bay of Brest
148 and in the Bay of Vilaine (in the Northern part of the Bay of Biscay) is observed by Poppeschi
149 et al. (2022). The impact of MHW on biology is even more studied than the cold counterpart.
150 Gomez and Souissi (2008) show the link between the heatwave of 2003 in the English
151 Channel and the abundance of dinoflagellates. Joint and Smale (2017) demonstrate a link
152 between MHW and microbial activity assemblage in the English Channel which controls
153 biogeochemical cycles in the ocean. The MHW of 2018 in the English Channel is present in
154 the literature for its mortality mass impact on mussels (Seuront et al., 2019), its link to fucoids
155 (Mieszkowska et al., 2020) or harmful phytoplankton blooms (Brown et al., 2022).
156 Predictions at the atmospheric scale point to an increase in the future of heatwaves in the Bay
157 of Biscay (Chust et al., 2011) and a decrease in marine fauna (Wethey and Woodin, 2022).

158

159 In this context, we aim to describe and explain the evolutions of the MHW over
160 summer and MCS over winter activity in the Northeast Atlantic and to investigate the regional
161 variability in three subregions: the English Channel, the Bay of Brest and the Bay of Biscay.
162 The analysis will rely on both *in situ* and satellite data to address MHW and MCS activity,
163 aiming to evaluate the impact of such events in coastal regions and in the open ocean. This
164 approach will allow us to evaluate the potential use of *in situ* measurements to detect,
165 characterize and understand such extreme events. In the last section of this paper, we focus on
166 the influence of the interannual atmospheric mode of variability involved in the occurrence of
167 MHW and MCS in the Northeast Atlantic by finding the atmospheric circulation occurring in
168 phase with most of the strongest events.

169

170

171 2. Material and methods

172

173 2.1 Satellite data

174

175 The global SST data used in this study results from a combination of different
176 observational platforms, including satellites, ships, buoys and Argo floats, provided by the
177 National Oceanic and Atmospheric Administration (Reynolds et al., 2007; Huang et al.,
178 2020). The data, hereafter OISST, have a daily temporal coverage for the 1982-2022 period
179 and are interpolated to a regular global grid of $1/4^\circ$ spatial resolution.

180

181

182 2.2 Buoy data

183

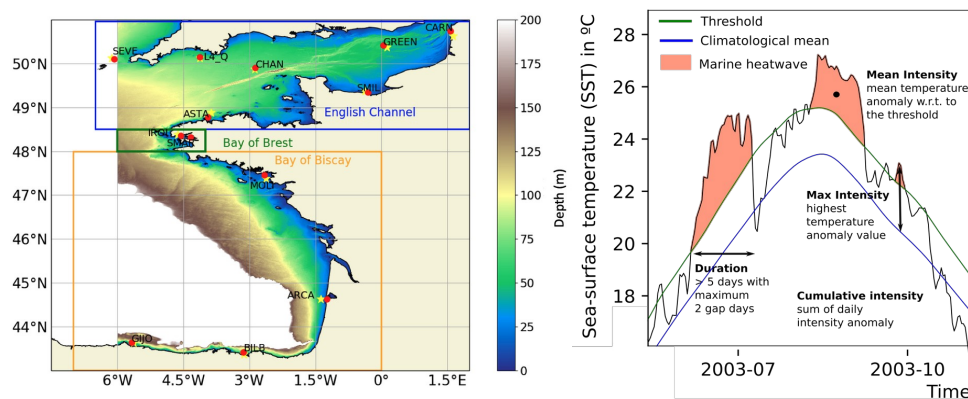
184 The *in situ* SST data are from autonomous coastal buoys that take continuous high-
185 frequency measurements from 10 minutes to 1 hour (Figure 1, left panel). These buoys are
186 from different European organizations, detailed below and in Table S1, covering the coastal
187 areas of the English Channel, the Bay of Brest and the Bay of Biscay.

188 The National Observation Infrastructure network (COAST-HF, www.coast-hf.fr)
189 operates 14 buoys taking measurements of several physical and biogeochemical data all
190 around French coasts. Among them, 7 buoys are used here and are located in the English
191 Channel - CARNot, SMILe and ASTAn; in the Bay of Brest - IROise and SMARt and in the
192 Bay of Biscay - MOLIt and ARCAchon. The Met Office (www.metoffice.gov.uk) manages
193 several buoys in each facade of England and also at offshore sites. The buoys used here are
194 located in the English Channel, on the South coast of England, SEVEN Stones; CHANnel and



5

195 GREENwich. The Western Channel Observatory (WCO,
 196 www.westernchannelobservatory.org.uk), situated within the western English Channel
 197 operates two oceanographic moorings. The station L4_Q located near the city of Plymouth,
 198 approximately 7 km offshore is used here. Puertos del Estado (www.puertos.es) operated two
 199 buoys along the Spanish coast: BILBao and GIJOn located in the Cantabrian Sea, both of
 200 them are used here.
 201



202
 203 Figure 1: (Left) Map of the study area including the whole domain as well as the three
 204 subregions which are the English Channel (in blue), the Bay of Brest (in green) and the Bay
 205 of Biscay (in orange). The buoys are represented by red dots and the satellite points are
 206 represented by yellow stars. (Right) Marine heatwave properties are defined as in Hobday et
 207 al., 2016.
 208
 209

210 2.3 Detection of MHW and MCS

211
 212 To detect marine temperature extreme anomalies, we use the definition of Hobday et
 213 al. (2016). First, a climatology over 40 years, from 1982 to 2022, is calculated from the
 214 OISST product. Then, we apply the 90th percentile on summers (JJAS) for MHW and the 10th
 215 on winters (DJFM) for MCS. Finally, a MHW (MCS) is detected if values are above (below)
 216 the threshold for at least 5 days. For *in situ* data, the same detection method is applied
 217 considering the climatology calculated from OISST products. Only seasons (summer or
 218 winter) with more than 80% of available data are analyzed.

219 To characterize MHW and MCS, we analyze parameters such as the number of events,
 220 the duration, the spatial extent and the cumulative intensity, defined as in Hobday et al. (2016)
 221 (Figure 1, right panel). We also explore an integrated indicator of these different parameters
 222 characterizing the marine temperature extreme events (MHW and MCS), called activity and
 223 defined by Simon et al. (2022). This indicator estimates for each grid point the cumulative
 224 combination of the mean intensity, the duration and the affected area of each extreme event
 225 within a specific time range. This activity metric accounts explicitly for the area, as in most
 226 SST products a grid cell area differs from one latitude to another and marine thermal events
 227 can expand over large areas.
 228

229
$$Activity = \sum_{EE \in Time\ Range} mean\ intensity_{EE} \cdot duration_{EE \cap Time\ Range} \cdot area_{EE}$$

230



6

231 Where $EE \in \text{time range}$, denotes the extreme event (EE) that occurs within the selected time
232 range; the mean intensity of EE (in $^{\circ}\text{C}$) is the mean temperature anomaly with respect to the
233 threshold of the event; duration $EE \cap \text{time range}$ (in days) is the duration of the event that
234 remains within the considered time range, and $area_{EE}$ (in km^2) is the area affected by the
235 discrete event. Time series involving the activity metric for a domain are calculated as the
236 mean of every grid cell considered. The activity for each station is computed in $^{\circ}\text{C.days}$
237 without considering the area influenced by the events as it can not be estimated from single
238 localized stations.

239 This method of detection and characterization of marine thermal extreme events is
240 performed over the whole domain of this study, referred to as the Northeast Atlantic (8°W to
241 2°E - 43°N to 51°N) and at each station where *in situ* observations are available. As
242 illustrated in Figure 1, 3 different subregions will be analyzed in detail, namely (i) the English
243 Channel (6.5°W to 2°E - 48.5°N to 51°N), (ii) the Bay of Brest (6°W to 4°W - 48°N to
244 48.5°N) and (iii) the Bay of Biscay (7°W to 0°W - 43°N to 48°N). This will allow us to
245 explore these regions separately and highlight regional patterns. Those three subregions can
246 be associated with three contrasted hydrodynamical regimes: macrotidal (English Channel),
247 semi-enclosed bay (Bay of Brest), mesotidal (Bay of Biscay; Charria et al., 2013).
248

249 3. Results

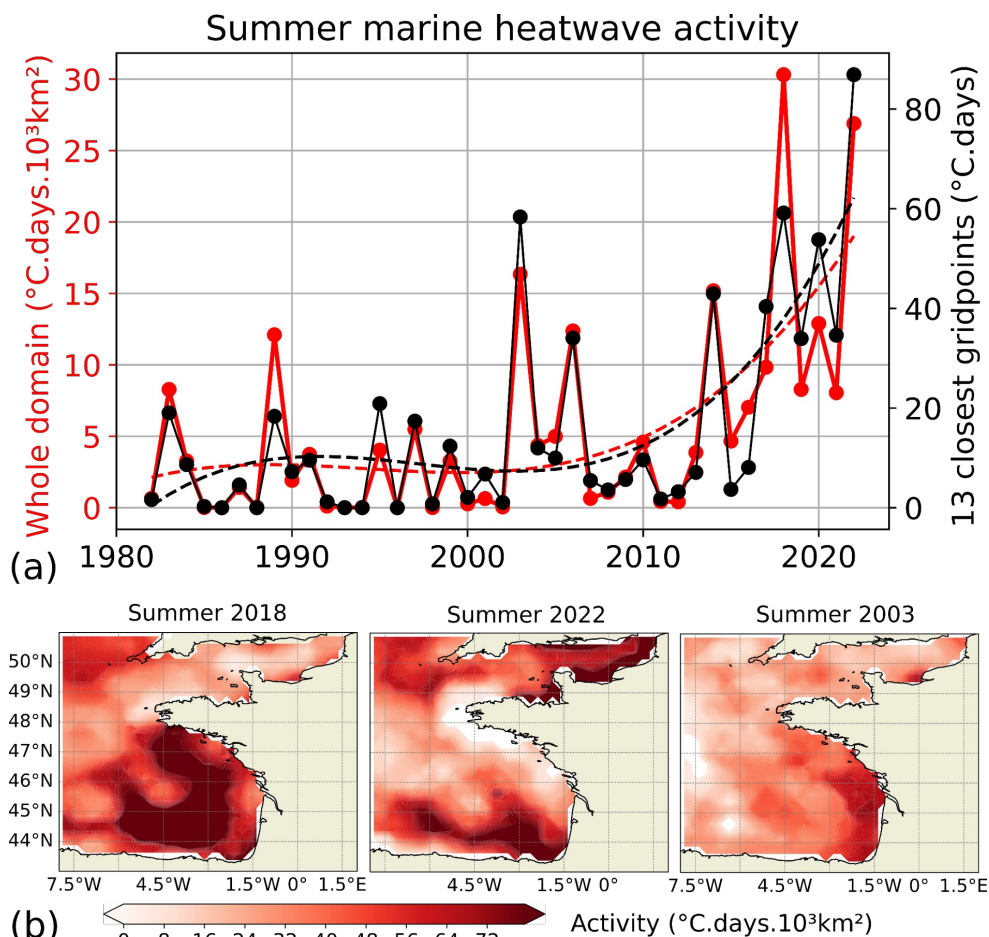
250 3.1 Evolution of marine heatwave activity

251 3.1.1. An integrated regional view

252
253
254
255 Marine heatwaves were detected over the Northeast Atlantic. The activity indicator
256 (Figure 2a) highlights two main periods in the MHWs dynamics. Before 2003, MHWs
257 activity remained moderate to weak with activity generally lower than $5^{\circ}\text{C.days.10}^3\text{ km}^2$
258 corresponding to 1.2 mean occurrences per summer with a mean duration limited to 8 days
259 (Figure 3). Only the summer of 1989 displayed strong MHWs activity (exceeding 10^4
260 $^{\circ}\text{C.days.10}^3\text{ km}^2$) before 2000. From 2003 onward, the activity increased over 30^4
261 $^{\circ}\text{C.days.10}^3\text{ km}^2$ for summers 2018 and 2022 associated with more than 2.5 mean occurrences lasting
262 around 20 days. The mean intensity remains quasi-steady during the whole period. The
263 interannual trend of the MHW summer activity for the whole domain is similar to the one
264 obtained for the average activity of the 13 grid cells closest to the buoy locations (black line
265 of Figure 2).
266
267



7

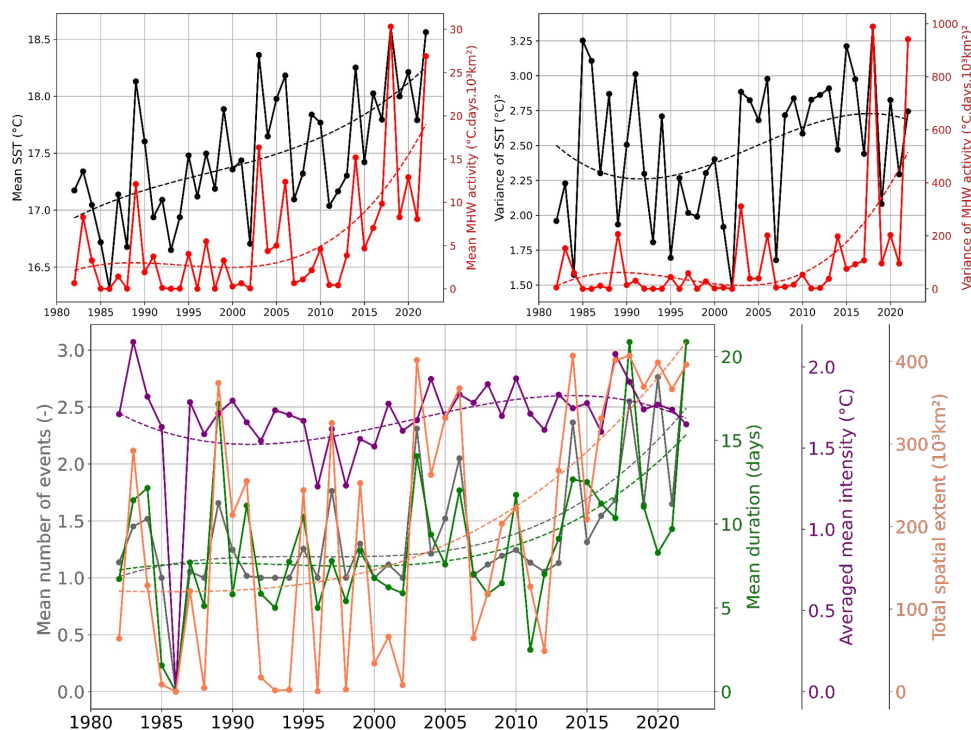


268
 269 Figure 2: (a) Times series of summer (JJAS) marine heatwaves mean activity in the Northeast
 270 Atlantic from OISST (red curves) and for the average of the 13 grid cells closest to the buoys
 271 from OISST (black curves). Dash lines represent the regression of a third-order polynomial of
 272 the solid line with the same color. (b) Summer (JJAS) activity (first row; in °C.days.10³ km²)
 273 for the top 3 summers in terms of activity in the Northeast Atlantic (from left to right).
 274

275 The three most active summers are 2018, 2022 and 2003 (Figure 2a). During 2018
 276 (Figure 2b), maximum activity is located in the Bay of Biscay over the outer continental shelf
 277 and the continental slope from the southern part of the Biscay. The marine heatwave is also
 278 extending to the North until the South of Brittany and is limited by the Ushant tidal front (Le
 279 Boyer et al., 2009; Müller et al., 2010) developed during summer. Regions of minimum
 280 activity during 2018 are West of French Brittany in the Ushant front region where tides are
 281 efficiently vertically mixing the water column. Similarly, the activity remains weak in the
 282 English Channel, as it is a macrotidal region. In terms of duration, longer events are observed
 283 in the Southern part of the Bay of Biscay exceeding 30 days (Figure S1). The 2022 summer is
 284 the second most active year for the whole domain, with over 25 °C.days.10³ km², and also the
 285 strongest in terms of marine activity over coastal regions as shown by the maximum value of
 286 the average activity near the 13 buoys considered (Figure 2a). Spatially, the English Channel
 287 and the North of Spain record the strongest MHWs activity while the French Brittany coast



288 has no occurrence over this year (Figure 2b). In the English Channel, the mean duration of the
 289 events was around 35 days (Figure S2) with localized events lasting more than 50 days
 290 (Figure S1). In Northern Spain, the duration of the events was around 20 days, however, they
 291 occurred very frequently over the summer with strong mean MHW intensities of around 2 °C
 292 (Figure S1). In 2003 (Figure 2c), the MHWs activity spatial distribution was different than in
 293 2018 and 2022. The activity is larger over the inner continental shelf along Western French
 294 coasts in the Bay of Biscay. This region is under the influence of main river plumes along this
 295 coast (Adour, Gironde and Loire rivers). During this year, river discharge has induced
 296 stratification (inducing faster warming of the surface mixed layer in regions of freshwater
 297 influence) and warmer waters from rivers suggest that observed MHW were sustained by an
 298 atmospheric event more centered over lands. By contrast, the number of events is larger in the
 299 Western English Channel but shorter and less intense than in the Bay of Biscay. These top
 300 three active summers highlight the interannual spatial variability of MHWs activity.
 301



302
 303 Figure 3: Time series of the mean (Top) and variance (Middle) of SST (black curve) and
 304 MHW activity (red curve) of summers (JJAS) over the Northeast Atlantic for the period 1982-
 305 2022. (Bottom) Mean properties of summer (JJAS) MHW in the Northeast Atlantic. The
 306 mean number of events (grey curve) is the number of events within the summer averaged over
 307 the domain. Mean duration (green curve) is the average duration of every event within the
 308 summer and domain. Averaged mean intensity (purple curve) is the average of the mean
 309 intensity of every event within the period and domain. Total spatial extent (orange curve) is
 310 the sum of each grid cell area where one or more events occur. If more than one MHW occurs
 311 on the same cell, only one grid cell area is taken into account. Dash lines represent the
 312 regression of a third-order polynomial of the solid line with the same color.
 313



314 The mean SST has been increasing over the 40 years with an approximately linear
315 trend, showing a mean warming of nearly 1.5 °C for the whole domain since 1982 (Figure 3).
316 Regionally, it is observed that the increase in the mean SST is almost yearly constant for the
317 Bay of Biscay region, and quadratic for the English Channel and Bay of Brest, where a
318 plateau is observed around 1995-2010 (Figure S2).

319 Over the Northeast Atlantic, the first 10 years and the 5 most recent years are
320 characterized by a decline in the SST variance, while around 1992-2017 an increase in the
321 spatial dispersion is observed. This interannual trend is similar to the ones observed for the
322 events' intensity, with the exception of the English Channel, showing a direct relationship
323 between the SST variance and the mean intensity of the MHW events. The mean MHW
324 activity and its variance, over 1982-2022, show two distinct phases (Figure 3). From the
325 beginning until 2005 the variation is weak, while after this year a strong positive trend is
326 observed. In the English Channel, Bay of Brest and Bay of Biscay, the mean SST is warming
327 and the variance is increasing, both contributing to the changes in the respective MHW
328 activity.

329 Contributing to this recent increase is primarily the sharp trend of the events' spatial
330 extent (~180 to 400 °C.days.10³ km²), followed by the rise of the number of events (1.2 to
331 2.5) and also their duration (7 to 15 days). One should note that, for the same number of
332 events, the events' spatial extent can differ depending on their spatial repartition, as in the
333 events' spatial extent only one grid cell area is taken into account when more than one event
334 occurs on the same grid. Furthermore, over the most recent years the mean number of events,
335 their mean duration and total spatial extent reached the maximum recorded values. Since
336 2017, the total spatial extent over the Northeast Atlantic has recorded consecutive high values,
337 exceeding 360 103 km². The summers of 2018, 2020 and 2022 recorded on average more than
338 2.5 events for almost all subregions, with events lasting on average more than 20 days in 2018
339 (Bay of Biscay) and 2022 (English Channel; Figure S2). The longest mean duration is seen in
340 the English Channel (35 days in summer 2022), the highest mean number of events occurred
341 in the Bay of Brest (2.7 in summer 2020) and the highest mean intensity is present in the Bay
342 of Biscay (2.2 °C in 2017; Figure S2).

343

344

345 3.1.2. Coastal MHW activity

346

347 The spatial heterogeneity of the MHWs occurrence and activity can influence the
348 impact of MHWs along the coastline. We then explore MHWs activity detected along the
349 coast from *in situ* observations compared with remotely sensed observations. Figure 4 shows
350 the activity detected for the whole Northeast Atlantic domain and in the three subregions
351 where long-term *in situ* observations exist. Linked with the whole domain activity (Figure 4a),
352 we observe an increase in the MHWs activity in the three subregions (Figure 4b, c, d). Similar
353 evolutions are observed when the satellite product OISST or coastal buoys are considered. In
354 the Bay of Brest, we also observe a similar increase but with larger activity in *in situ*
355 observation as the intensity of extreme is underestimated by the satellite in this semi-enclosed
356 bay. The use of *in situ* observation is limiting the length of the analyzed time series. However,
357 we can observe larger activity in recent years from both datasets. For most cases, similar most
358 active years are detected with *in situ* observations and satellite data.

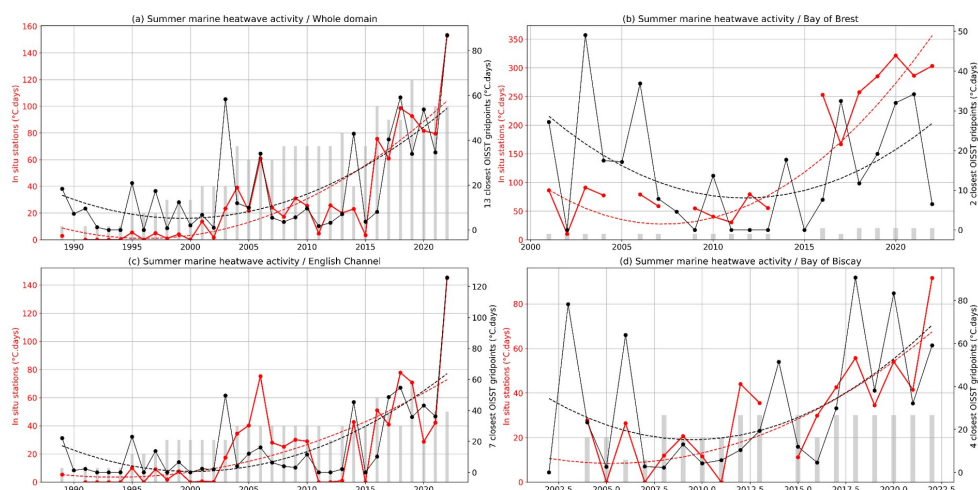
359

360 Considering coastal stations over the observed periods, we see a more pronounced
361 increase in MHW activity from 2010. The English Channel and the Bay of Biscay *in situ*
362 stations highlight the year 2022 as the most active year exceeding 140 °C.days. In the Bay of
363 Brest, the impact of the 2022 MHWs is less pronounced, in agreement with OISST
observation (Figure 2b) due to tidally driven vertical mixing.



10

364 When we compare MHW activity estimated from *in situ* stations and OISST product, values
 365 are generally larger from *in situ* stations. Those differences are explained by the
 366 underestimation of extreme temperatures in coastal regions in remotely sensed products.
 367
 368



369 Figure 4: Time series of summer (JJAS) marine heatwave mean activity (a) in the whole
 370 domain (Northeast Atlantic) and in three subregions: (b) Bay of Brest, (c) the English
 371 Channel, and (d) Bay of Biscay. The red curve represents the activity based on *in situ*
 372 observations. The black curve represents the activity based on OISST products for the closest
 373 non-masked points with *in situ* stations. Dash lines represent the regression of a third-order
 374 polynomial of the solid line with the same color. Grey bars are proportional to the number of
 375 considered *in situ* time series. MHW activity from *in situ* time series with less than 80% of
 376 observation during the analyzed season is not computed.
 377

378

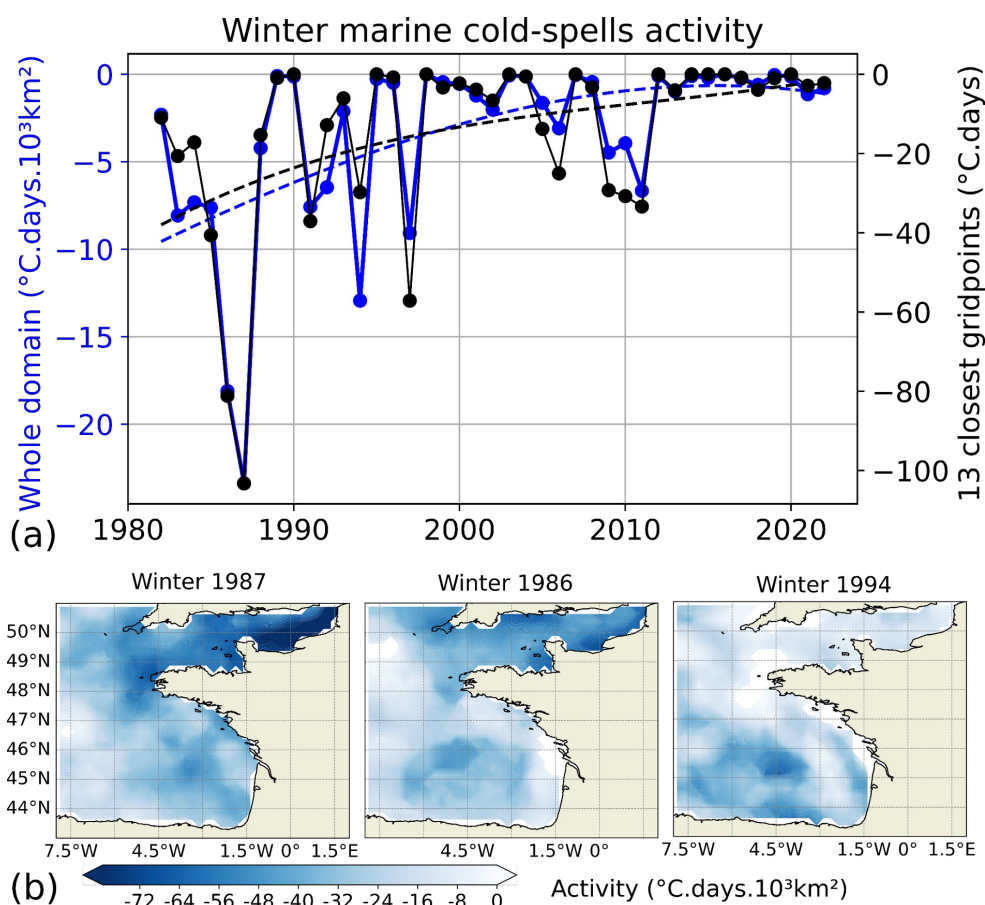
379 3.2 Evolution of marine cold-spell activity

380

381 3.2.1 An integrated regional view

382

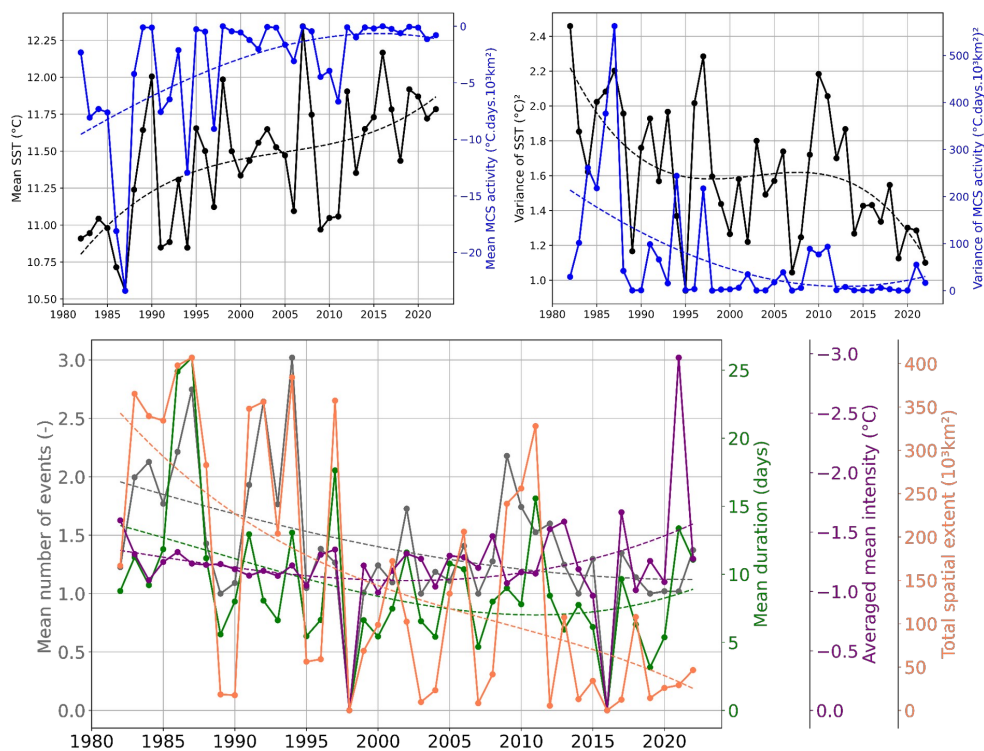
383



384
385 Figure 5: Same as Figure 2 but for MCS in winter (DJFM).
386

387 Figure 5 depicts winter MCS evolution for the whole domain over the last four
388 decades (1982-2022). MCS activities decrease linearly during the first half of the period,
389 showing almost no occurrences after 2000 with the exception of 2006 and 2009 to 2011. A
390 similar evolution is seen by considering the average of the 13 grid points closest to each *in*
391 *situ* station.

392
393 The three most active MCS occur in winter 1987 (-24 °C.days.10³.km²), 1986 (-18
394 °C.days.10³.km²) and 1994 (-13 °C.days.10³.km²). In the two coldest winters, MCSs were
395 dominant in the English Channel, especially off the Northern French Coast in winter 1987.
396 These two winters are characterized by long (~ 50 days) and intense (~ -2.5 °C anomalous
397 SST) and few events (~ 1 event; Figure S3). This region is subject to high turbulent mixing
398 generated by the tidal current, which could favor cold conditions. By contrast to these two
399 winters (1987 and 1986), winter 1994 featured strong marine cold-spells activity in the center
400 of the Bay of Biscay, due to numerous (~ 5 events) but moderate intensity (~ -1.3 °C) and
401 relatively short (20 days) events. The three winters 2009-2011 present very localized extreme
402 cold conditions along the coastal Armorican Shelf, and additionally in the English Channel
403 for 2011 (not shown).
404



405
406

407 Figure 6: Same as Figure 3 but in winter (DJFM) and MCS (blue curve)

408

409

410

411

412

413

414

415

416

The mean and variance evolution of SST and MCS activities, as well as the mean evolution of MCS properties (occurrence, duration, mean intensity and spatial extent) are presented over the whole domain (Figure 6) and separately for the English Channel, the Bay of Brest and the Bay of Biscay (Figure S4). Over the whole Northeast Atlantic domain, the SST mean increases and spatial dispersion (variance) decreases with both a plateau around 1995-2010, following the English Channel and the Bay of Biscay evolution. On the contrary, a steady increase in the mean SST and a nearly constant variance of SST is seen in the Bay of Brest.

417

418

419

420

421

422

The warmer winter seen over the whole domain and for the three subregions is consistent with the decrease of the extremely cold conditions, depicted by the mean MCS activity. The decrease in the mean MCS activity is controlled by the strong decrease in spatial extent (350 to 50 10³.km²), the moderate decrease in the number of events (2 to 1.2 events), and the small decrease in duration (13 to 9 days). The mean intensity does not show any trend (~ -1.5 °C).

423

424

425

426

427

428

429

The decrease of spatial dispersion (variance) of SST over the whole domain indicates a more uniform evolution which is explained by a dominant warming trend stronger for colder areas. Indeed, the relatively cold English Channel's temperature increased by 1.5 °C (from 9 °C to 10.5 °C) and the relatively warmer Bay of Biscay increased by 0.8 °C (from 11.8 °C to 12.6 °C) over the 1982-2022 period. This is reflected in the decrease in the variance of MCS activity. When considering individually the three subregions, localized enough to be under a similar trend, the variance also decreases, reflecting a decrease in MCS activity (Figure S4).



13

430 The decrease of variance is more pronounced for the English Channel than for the Bay of
431 Brest and Bay of Biscay. Therefore, mean SST warming and the variance changes both
432 contribute to the changes in MCS activity in the English Channel, Bay of Brest and Bay of
433 Biscay.

434 MCS activity generally follows the SST evolution, albeit with small differences.
435 Indeed, winter 1991 and 1994 have a similar mean SST (10.8 °C) but the MCS activity is
436 three times higher in 1994 than in 1991, driven by a higher number of events (3 instead of 2
437 events with similar duration, mean intensity and spatial extent).

438 Even if changes in winter occur in the Bay of Brest and Bay of Biscay, more drastic
439 changes are seen in the English Channel over the period 1982-2022. In the English Channel,
440 the trend of MCS shows at the beginning of the period, a mean occurrence of 2 events/winter,
441 lasting 15 days with a mean intensity of -1.5 °C over an area of 100 10³ km², followed by a
442 sharp decline ending to no detected MCS in the last four years (2019-2022). In the Bay of
443 Brest over the same period, MCS properties decrease from 1.5 events during 15 days at a
444 mean intensity of -1.4 °C over 11 10³ km² to 0.5 events during 8 days at a mean intensity of -
445 0.8 °C over 0.5 10³ km². Exceptional long events occurred in the winter of 1987 with a mean
446 duration of 55 days. In the Bay of Biscay, the marine cold-spells decline in occurrence (from
447 2 to 1 event), duration (from 11 to 9 days) and spatial extent (170 to 40 10³ km²) while the
448 mean intensity rises from -1.3 °C to -1.5 °C. The increase is explained by winter 2021, without
449 these events, the mean intensity would have been nearly constant around -1.3 °C. Indeed,
450 winter 2021 shows a small activity but the highest mean intensity (-3 °C over the whole
451 domain) which is explained by a localized event in the coastal area off South-West of France
452 with a maximum intensity of (-5.6 °C). Apart from a very intense and localized event in the
453 coastal area off South-West of France in winter 2021 and a very long event in the Bay of
454 Brest in winter 1987, severe marine cold-spells occurred predominantly in the English
455 Channel (winter 1987 and 1986).

456

457

458 3.2.2. Coastal MCS activity

459

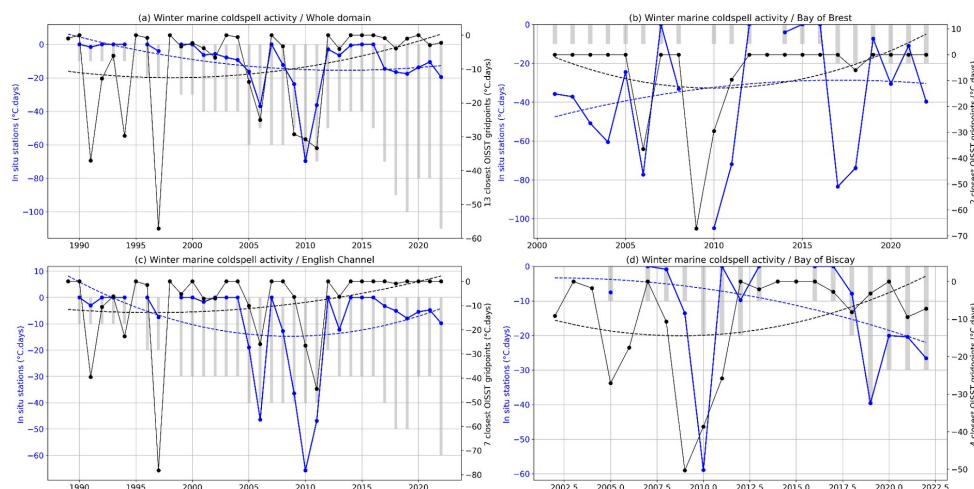
460 Along the coasts, MCS activity as determined by local buoys remains weaker than
461 MHW activity. As for the MHWs, MCS intensity is slightly underestimated in satellite
462 observations but evolutions are similar. From *in situ* observations from coastal stations, two
463 years can be highlighted due to their intense MCSs: 2006 and 2010 (Figure 7). The year 2010
464 is the most intense, in terms of MCSs. The mean activity is reaching -100 °C.day in the Bay of
465 Brest and around -60 °C.day in the Bay of Biscay and the English Channel. In 2006, the
466 activity was also important compared with other years: around -80 °C.day in the Bay of Brest
467 and around -50 °C.day in the English Channel. This extreme year 2006 was also unique with a
468 peak in MHW activity during the summer (Figure 4). Before the year 2000, only observed in
469 the English Channel from coastal stations, three other years reveal intense MCS activity:
470 1997, 1991, 1994 (from the most intense to the less active winter) from OISST data at the
471 closest point of *in-situ* data.

472 We do not detect a significant trend in the interannual evolution of MCS activity along
473 the coasts. For the Bay of Biscay and the Bay of Brest, it can be directly connected to the lack
474 of observation before 2000 when the largest MCS occurs. In the English Channel, the lack of
475 observation also explains the observed lack of trend. Indeed, only one time series was
476 available before 1995 and this station (GREENwich) is not detecting an important MCS
477 activity before 2000.



14

478
479



480
481

482 Figure 7: Same as Figure 4 but for MCS in winter (DJFM).

483

484 3.3 Associated atmospheric patterns

485

486

487

488

489

490

491

492

493

494

495

496

497

498

499

500

501

502

503

504

505

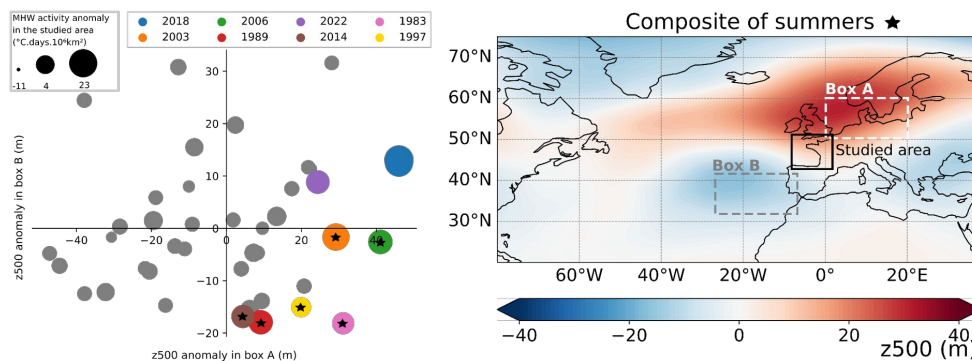
506

507

Apart from the long-term trend of increasing SST, we also see high interannual variability which is potentially connected with atmospheric forcing modes (Holbrook et al. 2019; Izquierdo et al., 2022a). Figure 8 presents the atmospheric circulation in the North Atlantic associated with strong interannual marine heatwaves in the Bay of Biscay and the English Channel. For each summer of the 1982-2022 period, MHW total activity anomaly in the studied area box (Northeast Atlantic) with respect to the third-order long-term trend (red dotted curved in Figure 2a) was computed. This anomaly represents the detrended or interannual MHW activity. Eight summers were identified as having high interannual activities (anomalous total activity exceeding a threshold of $4 \text{ } ^\circ\text{C}\cdot\text{days}\cdot 10^6\cdot\text{km}^2$, coloured marker in Figure 8 left panel). The year 2018 ($23 \text{ } ^\circ\text{C}\cdot\text{days}\cdot 10^6\cdot\text{km}^2$), 2003 ($17 \text{ } ^\circ\text{C}\cdot\text{days}\cdot 10^6\cdot\text{km}^2$) and 2006 ($12 \text{ } ^\circ\text{C}\cdot\text{days}\cdot 10^6\cdot\text{km}^2$) are the three strongest summers. Six out of these eight summers (all except 2018 and 2022) have an anomalous geopotential height at 500 hPa which is positive over Northern Europe (box A in Figure 8) and negative in the West of the Iberian Peninsula (box B in Figure 8). The composite of the anomalous geopotential height at 500 hPa for these six summers shows in the North Atlantic-Europe sector a positive summer NAO-like pattern, with a high over the Nordic sea and two lows over the Iberian Peninsula and Greenland. This overall result is not sensitive to small displacements of boxes (a few latitude and longitude degrees; not shown).



15



508
 509 Figure 8: (Left panel) Scatter plot of anomalous summer (JJAS) geopotential height at 500
 510 hPa (z500; in m) in box A versus the anomalous geopotential height at 500 hPa in box B with
 511 respect to the summer period 1982-2022. The size of the marker is proportional to the
 512 anomalous summer (JJAS) MHW total activity, calculated as the sum of all grid point activity
 513 in the studied area (in °C.days.10⁶.km²) with respect to the trend (red dotted curved in Figure
 514 2a). Markers are in color when this value exceeds 4 °C.days.10⁶.km² and the stars are
 515 indicated when markers in color are in the lower-right “cluster” of the graph. (Right panel)
 516 Composites of summers (JJAS) marked with stars in the left panel of the anomalous
 517 geopotential height at 500 hPa (m) with respect to the summer period 1982-2022. Box A is
 518 the domain 0°E to 20°E-50°N to 60°N and box B is the domain 33°W to 13°W - 31°N to
 519 41°N.

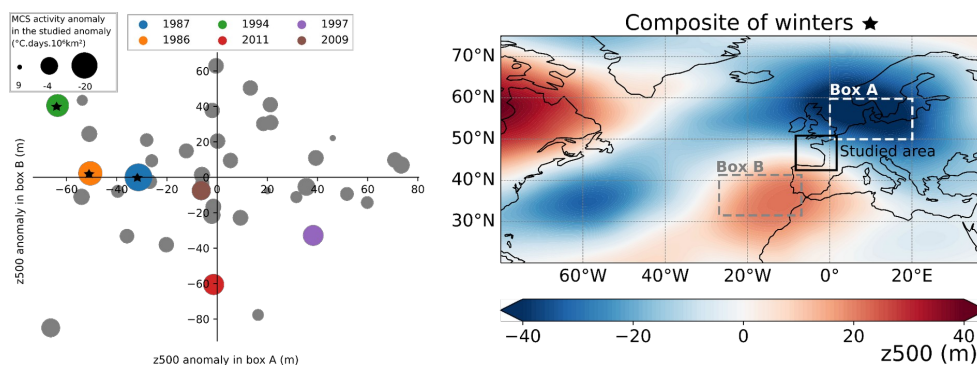
520
 521 Summer (JJAS) 2018 has the strongest anomalous MHW activity in the Northeast
 522 Atlantic but, at the difference to the six next summers in the ranking of detrended MHW
 523 activity, does not present a decrease in the geopotential height at 500 hPa in the West of
 524 Iberian Peninsula (box B). A broad high-pressure system in the North Atlantic-European
 525 sector is seen (including box A), except in the Eastern Mediterranean and up to 60°N where a
 526 low occurs (Figure S5). This response in box B for summer 2018 is primarily due to late
 527 summer (August and September) atmospheric circulation (Figure S5). These months have a
 528 minor contribution to marine heatwave total activity for the whole summer (JJAS; Figure S6).
 529 When considering the month of June, with 2018 MHW peaks (Figure S6), the North Atlantic
 530 shows a positive summer NAO regime, similar to the next six summers' highest marine
 531 heatwave activity. This analysis demonstrates that MHW in the Northeast Atlantic is closely
 532 associated with a high-pressure system over Northern Europe, and a low off the Iberian
 533 Peninsula, resembling the positive phase of the summer NAO. By performing this analysis
 534 with SST instead of the MHW activity, we obtain similar results, albeit with a less extended
 535 high over Northern Europe (Figure S7).

536

537



16



538

539

540

541

542

Figure 9: Same as Figure 8 but for marine cold-spells in winter (DJFM). Marine cold-spells anomalies are calculated with respect to the third-order trend (blue dotted curved in Figure 5). Markers are in color when this value is below $-4 \text{ }^{\circ}\text{C.days.10}^6.\text{km}^2$ and stars are indicated when markers in color are in the upper-left section of the graph.

543

544

545

546

547

548

549

550

551

552

553

554

555

Regarding MCS, the three highest detrended marine cold-spells activities are winter 1987 ($-20 \text{ }^{\circ}\text{C.days.10}^6.\text{km}^2$), 1986 ($-13 \text{ }^{\circ}\text{C.days.10}^6.\text{km}^2$) and 1994 ($-10 \text{ }^{\circ}\text{C.days.10}^6.\text{km}^2$; Figure 9). These three most active winters are in the same “cluster”, with an anomalous geopotential height at 500 hPa negative over Northern Europe and positive in the West of the Iberian Peninsula. Composite of the anomalous geopotential height at 500 hPa for these three winters shows in the North Atlantic-Europe sector a broad and strong low in Northern Europe, a weaker low-pressure system sitting in the Northwest Atlantic, and two highs off the Iberian Peninsula and over the Hudson Bay. This analysis suggests that extreme MCS in the Northeast Atlantic might be closely associated with a low over Northern Europe and a high off the Iberian Peninsula. By performing this analysis with SST instead of the MCS activity (Figure S8), the result are sparse, showing only winter 1986 as strong anomalous cold SST linked to an anomalous geopotential height at 500 hPa over Northern Europe and positive in the West of the Iberian Peninsula.

556

557

558

559

560

561

When comparing the anomalous geopotential height conditions for the most intense summer MHWs and winter MCS, we see that the geopotential height conditions are somehow opposite, although the amplitude is stronger for winter, consistent with stronger climatology (Folland et al., 2019). However, while summer MHW are associated with a positive summer NAO, winter MCSs do not present a negative winter NAO general pattern.

562

4. Discussion

563

564

565

566

567

568

569

570

571

572

573

In the Northeast Atlantic, an increase in the MHW activity and a decrease in MCS activity were observed. Interannual changes confirm that general large scale trends (Oliver et al., 2018; Schlegel et al., 2021) are also observed in regions where the coastal hydrodynamics could limit the impact due to active vertical mixing processes (*e.g.* barotropic and internal tides, wind-driven mixing in shallow waters).

The most active summer MHW analyzed over the Northeast Atlantic and in the period 1982-2022 occurred in the Bay of Biscay (2018) and the most active winter MCS occurred in the English Channel (1987). This is consistent with Schlegel et al. (2021) who found that the maximum intensity of MHW dominates MCS in the Bay of Biscay, and vice versa in the English Channel. Along the coasts, the maximum of MHW activity is detected in 2022 in the



574 English Channel which might be related to the summer European heatwaves recorded
575 (ECMWF, 2022; Savu, 2022).

576 In the Bay of Biscay, we see a linear warming rate in summer since the beginning of
577 the studied period. This is in accordance with DeCastro et al. (2009) which shows an
578 accelerated warming rate since the 1970s, based on data from 1854-2006. Mean SST together
579 with SST variance increase justify the rise of MHW. This increase of MHW is consistent with
580 Izquierdo et al. (2022a) who determined more precisely an equal contribution of each of these
581 two factors for the South coast of the Bay of Biscay. Besides, we found a positive trend for
582 the MHW activity parameter using both satellite data and the 4 buoys in the Bay of Biscay,
583 and for the duration and occurrence using satellite data. The trends are quasi-similar
584 considering only the two buoys on the South coast of the Bay of Biscay (GIJO and BILB) and
585 the two on the West coast of the Bay of Biscay (ARCA and MOLI; not shown) and are
586 marked by the high activity present in the more recent summers. This evolution in the
587 occurrence and duration of MHW was not seen in Izquierdo et al. (2022b) using two buoys in
588 the South coastal Bay of Biscay over the period 1998-2018, which could be explained by
589 local process or studied season (March to August).

590
591 The results from *in situ* and satellite datasets for each of the studied regions are quite
592 in agreement, albeit the satellite underestimates the amplitude of activity for both MHW and
593 MCS. Conversely, Izquierdo et al. (2022a) found an overestimation of the MHW using
594 satellites compared to *in situ* in the coastal upwelling region South of the Bay of Biscay,
595 which might be related to local processes. The satellite's coarse resolution mostly (i) smooths
596 small-scale and short events and (ii) interpolates with offshore regions, having greater thermal
597 inertia (Marin et al., 2021) which can lead to the overestimation of the duration of events and
598 the underestimation of the intensity. However, we show that coastal *in situ* stations distributed
599 along the Northeast Atlantic coasts allow the detection of large-scale evolutions of MHW and
600 MCS activity. Analyzed locally, they can also inform on evolutions related to local
601 hydrodynamics.

602
603 Internal variability of winter MCS is related to low pressure over Northern Europe and
604 a high-pressure West of the Iberian Peninsula for three (1987, 1986 and 1994) out of the six
605 most intense events. Among other strong interannual MCS, winter 2011 does not present this
606 pattern but could have been generated by a cold air outbreak brought by a ridge over
607 Greenland (Norris et al., 2013). A relation at an interannual timescale could exist between
608 MCS (Figure 7, middle panel) and extreme low-salinity events (Poppeschi et al., 2021) in
609 winter in the Bay of Brest, as, using the same *in situ* buoys (COAST-HF-Iroise from 2000-
610 2018), two out of the four most severe low-salinity events are concomitant with marine cold-
611 spells (winter 2001 and 2007). These extreme events could be both influenced by intense mid-
612 latitude depressions, but river discharges are also an important driver in this region. Unlike
613 MHW (Figure 2), extreme cold conditions occurred several winters in a row: three in 2009-
614 2011 and two in 1986-1987. This might be explained by the re-emergence of cold water
615 originating from the previous winter, as for the 2013-2016 north Atlantic cold Blob (Duchez
616 et al., 2016a; Josey et al., 2018; Schlegel et al., 2021).

617
618
619 Summer 2018 presents the most active MHW in the Northeast Atlantic for the period
620 1982-2022, consistent with the reported warmer SST (+1 to +3 °C above the long-term
621 climatology) the same summer in the proximity of the United Kingdom (McCarty et al.,
622 2019). On the continental side, this summer was also recorded as the hottest in the United
623 Kingdom since 1884 (McCarty et al., 2019) and one of the hottest over northwestern Europe



18

624 (Met Office, 2018; Météo-France, 2018). On top of the underlying warming climate forcing
625 (Vogel et al., 2019; Yiou et al., 2020), this extreme continental warm conditions in 2018 have
626 been previously reported as a consequence of the positive summer NAO anomalies combined
627 with elevated SST (McCarty et al., 2019) or combined with stationary Rossby waves in
628 synoptic anomalies (Drouard et al., 2019; Kornhuber et al., 2019). More generally, the
629 positive phase of the summer NAO is associated with warm anomalies from the West of the
630 United Kingdom to the Baltic (Folland et al., 2009). Our findings on the ocean side
631 corroborate the continental counterpart as extremely warm conditions in the Bay of Biscay
632 and the English Channel are likely associated with positive summer NAO, consistent with the
633 result of Holbrook et al. (2019).

634

635 In the future and under increasing greenhouse gas concentrations, climate models
636 predict that the ocean surface in the Bay of Biscay and the English Channel will continue to
637 warm (Fox-Kemper et al., 2021) and a trend toward a positive summer NAO pattern (Faranda
638 et al., 2019). Both these effects imply the long-term likelihood of increased MHW in the
639 Northeast Atlantic, but to what extent are the long-term and the interannual variability
640 contributions remain to be shown. Also, the role of large-scale ocean circulation features,
641 such as the Shelf Edge Current (Alheit et al., 2019) or Iberian Poleward Current (Charria et
642 al., 2013), and the importance of remote large-scale climate modes of variability, such as the
643 Indian Ocean Dipole (Holbrook et al., 2019) in amplifying or suppressing MHW occurrences
644 in the Bay of Biscay and English Channel would need specific investigation. Along the
645 coasts, the role of main river inflow at the land-sea continuum can also lead to specific
646 answers on the coastal ocean to future climate evolutions.

647

648

649 5. Conclusions

650

651 The activity metric, a combination of the properties of marine extreme events, shows a
652 positive trend for summer marine heatwaves in the Northeast Atlantic (since 2000 and more
653 pronounced since 2010) and in the three subregions, the English Channel, the Bay of Brest
654 and the Bay of Biscay for both *in situ* and satellite data. This is explained by both a mean and
655 variance SST increase. Conversely, a decrease in marine cold-spell activity was detected, with
656 almost no events after 2000, more clearly with the satellite data due to the longest time series
657 (40 years) compared with the *in situ* (20 to 30 years). These changes are fast for the three
658 subregions, with the English Channel being the subregion with the more drastic growth.

659 In the Northeast Atlantic, marine heatwaves are more frequent, longer, and extend over larger
660 areas, while the opposite is seen for marine cold-spells. For both MHWs and MCSs, the mean
661 intensity shows only weak changes over the last four decades.

662 Moreover, we found that the satellite dataset used is in good accordance with *in situ* data in
663 the Northeast Atlantic, except for the fact that satellites underestimate the amplitude of both
664 hot summer and cold winter marine extreme events in the coastal areas. The implemented *in*
665 *situ* stations appear as a well-designed observing system to detect the long-term evolution of
666 MHW and MCS activity and to document local features related to coastal hydrodynamics.

667

668

669 MHWs activity is particularly high in 2018 and 2022 through two different situations.
670 The year 2018 is characterized by a large extent of MHWs in the Bay of Biscay with long
671 events in the South of the Bay and intense events in the Armorican Shelf. The summer of
672 2022 features long MHWs mainly in the English Channel. MCSs activity is the highest in
673 1986 and 1987 due to long and intense events in the English Channel.



19

674 Our findings show that summers with strong marine heatwave activity due to internal
675 variability (after removing the trend) in Northeast Atlantic have often been associated with a
676 ridge over the northern Europe sea and a trough West of the Iberian Peninsula; the opposite
677 situation is seen for MCSs. In the case of MHW, the wide atmospheric pattern resembles the
678 positive phase of the summer NAO. We caution that the proposed connection does not
679 necessarily indicate causal links but these relations can provide indications of drivers.

680

681 Despite contrasted hydrodynamical regimes (meso- and macro-tidal) and circulation
682 (shallow water under freshwater influence, shelf circulation, active sub-mesoscale), the
683 Northeast Atlantic region displays similar changes in MHW and MCS activity between
684 coastal and open ocean regions. Those changes need to be anticipated to mitigate the impacts
685 on coastal ecosystems.

686

687 Acknowledgements

688 This work was partially supported by national funds through FCT (Fundação para a Ciência e
689 a Tecnologia, Portugal) through project ROADMAP (JPIOCEANS/0001/2019). It is also
690 funded by the regional project (Contrat Plan Etat-Region) ObsOcean/ROEC-ILICO and the
691 regional COXTCLIM project funded by the Loire-Brittany Water Agency, the Brittany
692 region, and Ifremer. We thank Oregan Segalen for fruitful discussions. We thank Tim Smyth
693 for providing data from Western Channel Observatory. We acknowledge the COAST-HF
694 (<http://www.coast-hf.fr>) national observing network component of the National Research
695 Infrastructure ILICO.

696

697 Declaration of competing interest

698 The authors declare that they have no known competing financial interests or personal
699 relationships that could have appeared to influence the work reported in this paper.

700

701

702 References

703

704 Alheit, J., Gröger, J., Licandro, P., McQuinn, I. H., Pohlmann, T., & Tsikliras, A. C. (2019).
705 What happened in the mid-1990s? The coupled ocean-atmosphere processes behind climate-
706 induced ecosystem changes in the Northeast Atlantic and the Mediterranean. *Deep Sea*
707 *Research Part II: Topical Studies in Oceanography*, 159, 130-142.
708 <https://doi.org/10.1016/j.dsr2.2018.11.011>

709

710 Barnston, A. G., & Livezey, R. E. (1987). Classification, seasonality and persistence of low-
711 frequency atmospheric circulation patterns. *Monthly weather review*, 115(6), 1083-1126.
712 <https://doi.org/10.1175/1520-0493>



20

- 713 Brown Ross, A., Lilley, M. K. S., Shutler, J., Widdicombe, C., Rooks, P., McEvoy, A.,
714 Torres, R., Artioli, Y., Rawle, G., Homyard, J., Tyler, C. R., & Lowe, C. (2022). Harmful
715 Algal Blooms and their impacts on shellfish mariculture follow regionally distinct patterns of
716 water circulation in the western English Channel during the 2018 heatwave. *Harmful Algae*,
717 *111*(December 2021), 102166. <https://doi.org/10.1016/j.hal.2021.102166>
- 718 Charria, G., Lazure, P., Le Cann, B., Serpette, A., Reverdin, G., Louazel, S., Batifoulier, F.,
719 Dumas, F., Pichon, A., & Morel, Y. (2013). Surface layer circulation derived from
720 Lagrangian drifters in the Bay of Biscay, *Journal of Marine Systems*, *109*, 60–76.
721 <https://doi.org/10.1016/j.jmarsys.2011.09.015>
- 722 Chust, G., Borja, Á., Caballero, A., Irigoien, X., Sáenz, J., Moncho, R., Marcos, M., Liria, P.,
723 Hidalgo, J., Valle, M., & Valencia, V. (2011). Climate change impacts on coastal and pelagic
724 environments in the southeastern Bay of Biscay. *Climate Research*, *48*(2–3), 307–332.
725 <https://doi.org/10.3354/cr00914>
- 726 Crisp, D. J. (1964). The Effects of the Severe Winter of 1962-63 on Marine Life in Britain.
727 *Journal of Animal Ecology*, *33*(1), 165-210, <https://www.jstor.org/stable/2355>
- 728 Darmaraki, S., Somot, S., Sevault, F., & Nabat, P. (2019). Past Variability of Mediterranean
729 Sea Marine Heatwaves. *Geophysical Research Letters*, *46*(16), 9813–9823.
730 <https://doi.org/10.1029/2019GL082933>
- 731 DeCastro, M., Gómez-Gesteira, M., Alvarez, I., & Gesteira, J. L. G. (2009). Present warming
732 within the context of cooling–warming cycles observed since 1854 in the Bay of Biscay.
733 *Continental Shelf Research*, *29*(8), 1053-1059. <https://doi.org/10.1016/j.csr.2008.11.016>
734
- 735 Deser, C., Alexander, M. A., Xie, S. P., & Phillips, A. S. (2010). Sea surface temperature
736 variability: Patterns and mechanisms. *Annual review of marine science*, *2*, 115-143.
737
- 738 Drouard, M., Kornhuber, K., & Woollings, T. (2019). Disentangling dynamic contributions to
739 summer 2018 anomalous weather over Europe. *Geophysical Research Letters*, *46*(21), 12537-
740 12546. <https://doi.org/10.1029/2019GL084601>
- 741 ECMWF (2022). Update on European heatwave of July 2022 (available at:
742 www.ecmwf.int/en/about/media-centre/focus/2022/update-european-heatwave-july-2022)
- 743 Faranda, D., Alvarez-Castro, M. C., Messori, G., Rodrigues, D., & Yiou, P. (2019). The
744 hamman effect or how a warm ocean enhances large scale atmospheric predictability. *Nature*
745 *communications*, *10*(1), 1-7. <https://doi.org/10.1038/s41467-019-09305-8>
- 746 Folland, C. K., Knight, J., Linderholm, H. W., Fereday, D., Ineson, S., & Hurrell, J. W.
747 (2009). The summer North Atlantic Oscillation: past, present, and future. *Journal of Climate*,
748 *22*(5), 1082-1103.



21

- 749 Fox-Kemper, B., H.T. Hewitt, C. Xiao, G. Aðalgeirsdóttir, S.S. Drijfhout, T.L. Edwards, N.R.
750 Golledge, M. Hemer, R.E. Kopp, G. Krinner, A. Mix, D. Notz, S. Nowicki, I.S. Nurhati, L.
751 Ruiz, J.-B. Sallée, A.B.A. Slangen, & Y. Yu, (2021). Ocean, Cryosphere and Sea Level
752 Change. In *Climate Change 2021: The Physical Science Basis. Contribution of Working*
753 *Group I to the Sixth Assessment Report of the Intergovernmental Panel on Climate Change*
754 [Masson-Delmotte, V., P. Zhai, A. Pirani, S.L. Connors, C. Péan, S. Berger, N. Caud, Y.
755 Chen, L. Goldfarb, M.I. Gomis, M. Huang, K. Leitzell, E. Lonnoy, J.B.R. Matthews, T.K.
756 Maycock, T. Waterfield, O. Yelekçi, R. Yu, and B. Zhou (eds.)]. Cambridge University Press,
757 Cambridge, United Kingdom and New York, NY, USA, 1211–1362. [https://doi.org/](https://doi.org/10.1017/9781009157896.011)
758 [10.1017/9781009157896.011](https://doi.org/10.1017/9781009157896.011)
759
- 760 Frölicher, T. L., Fischer, E. M., & Gruber, N. (2018). Marine heatwaves under global
761 warming. *Nature*, 560(7718), 360-364. <https://doi.org/10.1038/s41586-018-0383-9>
- 762 Frölicher, T., & Laufkötter, C. (2018). Emerging risks from marine heat waves. *Nature*
763 *Communications*, 9(1), 2015–2018. <https://doi.org/10.1038/s41467-018-03163-6>
- 764 Gómez, F., & Souissi, S. (2008). The impact of the 2003 summer heat wave and the 2005 late
765 cold wave on the phytoplankton in the north-eastern English Channel. *Comptes Rendus -*
766 *Biologies*, 331(9), 678–685. <https://doi.org/10.1016/j.crv.2008.06.005>
- 767 Guinaldo, T., Picart, S. S., & Roquet, H. (2022). Response of the sea surface temperature to
768 heatwaves during the France 2022 meteorological summer. *EGUsphere*, 1-18.
769 <https://doi.org/10.5194/egusphere-2022-1119>
- 770 Hobday, A. J., Alexander, L. V., Perkins, S. E., Smale, D. A., Straub, S. C., Oliver, E. C. J.,
771 Benthuyzen, J. A., Burrows, M. T., Donat, M. G., Feng, M., Holbrook, N. J., Moore, P. J.,
772 Scannell, H. A., Sen Gupta, A., & Wernberg, T. (2016). A hierarchical approach to defining
773 marine heatwaves. *Progress in Oceanography*, 141, 227–238.
774 <https://doi.org/10.1016/j.pocean.2015.12.014>
775
- 776 Holbrook, N. J., Scannell, H. A., Sen Gupta, A., Benthuyzen, J. A., Feng, M., Oliver, E. C.,
777 Alexander, L., Burrows, M., Donat, M., Hobday, A., Moore, P., Perkins-Kirkpatrick, S.,
778 Smale, D., Straub, S., & Wernberg, T. (2019). A global assessment of marine heatwaves and
779 their drivers. *Nature Communications*, 10(1), 1-13. [https://doi.org/10.1038/s41467-019-](https://doi.org/10.1038/s41467-019-10206-z)
780 [10206-z](https://doi.org/10.1038/s41467-019-10206-z)
781
- 782 Huang, B., C. Liu, V. Banzon, E. Freeman, G. Graham, B. Hankins, T. Smith, and H.-M.
783 Zhang, 2020: Improvements of the Daily Optimum Interpolation Sea Surface Temperature
784 (DOISST) Version 2.1, *Journal of Climate*, 34, 2923-2939. doi: 10.1175/JCLI-D-20-0166.
785 (Accessed on 20-07-2021)
- 786 Hurrell, J. W., Kushnir, Y., Ottersen, G., & Visbeck, M. (2003). An overview of the North
787 Atlantic oscillation. *Geophysical Monograph-American Geophysical Union*, 134, 1-36.
788 <https://doi.org/10.1029/134GM01>



22

789 Izquierdo, P., Rico, J. M., Taboada, F. G., González-Gil, R., & Arrontes, J. (2022a).
790 Characterization of marine heatwaves in the Cantabrian Sea, SW Bay of Biscay. *Estuarine,*
791 *Coastal and Shelf Science*, 274(June). <https://doi.org/10.1016/j.ecss.2022.107923>

792 Izquierdo, P., Taboada, F. G., González-Gil, R., Arrontes, J., & Rico, J. M. (2022b).
793 Alongshore upwelling modulates the intensity of marine heatwaves in a temperate coastal sea.
794 *Science of the Total Environment*, 835(February).
795 <https://doi.org/10.1016/j.scitotenv.2022.155478>

796 Joint, I., & Smale, D. A. (2017). Marine heatwaves and optimal temperatures for microbial
797 assemblage activity. *FEMS Microbiology Ecology*, 93(2), 1–9.
798 <https://doi.org/10.1093/femsec/fiw243>

799 Kornhuber, K., Osprey, S., Coumou, D., Petri, S., Petoukhov, V., Rahmstorf, S., & Gray, L.
800 (2019). Extreme weather events in early summer 2018 connected by a recurrent hemispheric
801 wave-7 pattern. *Environmental Research Letters*, 14(5), 054002.
802 <https://doi.org/10.1088/1748-9326/ab13bf>
803

804 Le Boyer, A., Cambon, G., Daniault, N., Herbette, S., Le Cann, B., Marie, L., & Morin, P.
805 (2009). Observations of the Ushant tidal front in September 2007. *Continental Shelf Research*,
806 29(8), 1026-1037.
807

808 Lorenzo, M. N., Taboada, J. J., & Gimeno, L. (2008). Links between circulation weather
809 types and teleconnection patterns and their influence on precipitation patterns in Galicia (NW
810 Spain). *International Journal of Climatology: A Journal of the Royal Meteorological Society*,
811 28(11), 1493-1505. <https://doi.org/10.1002/joc.1646>
812

813 Marin, M., Feng, M., Phillips, H. E., & Bindoff, N. L. (2021). A global, multiproduct analysis
814 of coastal marine heatwaves: Distribution, characteristics, and long-term trends. *Journal of*
815 *Geophysical Research: Oceans*, 126(2), e2020JC016708.
816

817 McCarthy, M., Christidis, N., Dunstone, N., Fereday, D., Kay, G., Klein-Tank, A., Lowe, J.,
818 Petch, J., Scaife, A., & Stott, P. (2019). Drivers of the UK summer heatwave of 2018.
819 *Weather*, 74(11), 390-396. <https://doi.org/10.1002/wea.3628>

820 Met Office (2018). Summer 2018.
821 [https://www.metoffice.gov.uk/binaries/content/assets/metofficegovuk/pdf/weather/learn-](https://www.metoffice.gov.uk/binaries/content/assets/metofficegovuk/pdf/weather/learn-about/uk-past-events/interesting/2018/summer-2018---met-office.pdf)
822 [about/uk-past-events/interesting/2018/summer-2018---met-office.pdf](https://www.metoffice.gov.uk/binaries/content/assets/metofficegovuk/pdf/weather/learn-about/uk-past-events/interesting/2018/summer-2018---met-office.pdf)

823 Météo-France (2018). Bilan climatique de l'été 2018.
824 <https://meteofrance.fr/sites/meteofrance.fr/files/files/editorial/Bilan-climatique-annee2018.pdf>
825

826 Mieszkowska, N., Burrows, M., & Sugden, H. (2020). Impacts of climate change on intertidal
827 habitats, relevant to the coastal and marine environment around the UK. *MCCIP Science*
828 *Review 2020*, 256-271. <https://doi.org/10.14465/2020.arc12.ith>



23

829 Müller, H., Blanke, B., Dumas, F., & Mariette, V. (2010). Identification of typical scenarios
830 for the surface Lagrangian residual circulation in the Iroise Sea. *Journal of Geophysical*
831 *Research: Oceans*, 115(C7).

832 Norris, J., Vaughan, G., & Schultz, D. M. (2013). Snowbands over the English Channel and
833 Irish Sea during cold-air outbreaks. *Quarterly Journal of the Royal Meteorological Society*,
834 139(676), 1747-1761. <https://doi.org/10.1002/qj.2079>

835 Oliver, E. C., Donat, M. G., Burrows, M. T., Moore, P. J., Smale, D. A., Alexander, L. V., ...
836 & Wernberg, T. (2018). Longer and more frequent marine heatwaves over the past century.
837 *Nature communications*, 9(1), 1-12.

838 Oliver, E. C. J., Burrows, M. T., Donat, M. G., Sen Gupta, A., Alexander, L. V., Perkins-
839 Kirkpatrick, S. E., Benthuysen, J. A., Hobday, A. J., Holbrook, N. J., Moore, P. J., Thomsen,
840 M. S., Wernberg, T., & Smale, D. A. (2019). Projected Marine Heatwaves in the 21st Century
841 and the Potential for Ecological Impact. *Frontiers in Marine Science*, 6(December), 1–12.
842 <https://doi.org/10.3389/fmars.2019.00734>

843

844 Plecha, S., & Soares, P. M. M. (2020) Global marine heatwave events using the new CMIP6
845 multi-model ensemble: from shortcomings in present climate to future projections,
846 *Environmental Research Letters*, 15 (12), 124058. <https://doi.org/10.1088/1748-9326/abc847>

847 Plecha, S. M., Soares, P. M. M., Silva-Fernandes, S. M., & Cabos, W. (2021). On the
848 uncertainty of future projections of Marine Heatwave events in the North Atlantic Ocean.
849 *Climate Dynamics*, 56, 2027–2056. <https://doi.org/10.1007/s00382-020-05529-3>

850 Poppeschi, C., Charria, G., Goberville, E., Rimmelin-Maury, P., Barrier, N., Petton, S.,
851 Unterberger, M., Grossteffan, E., Repecaud, M., Quemener, L., Theetten, S., Le Roux, J.-F. &
852 Tréguer, P. (2021). Unraveling salinity extreme events in coastal environments: A winter
853 focus on the bay of brest. *Frontiers in Marine Science*, 8, 705403.
854 <https://doi.org/10.3389/fmars.2021.705403>

855

856 Poppeschi, C., Charria, G., Daniel, A., Verney, R., Rimmelin-Maury, P., Retho, M.,
857 Goberville, E., Grossteffan, E., & Plus, M. (2022). Interannual variability of the initiation of
858 the phytoplankton growing period in two French coastal ecosystems. *Biogeosciences*, 19,
859 5667–5687. <https://doi.org/10.5194/bg-19-5667-2022>

860

861 Reynolds R W, Smith T M, Liu C, Chelton D B, Casey K Sand Schlap M G 2007 Daily high-
862 resolution-blended analyses for sea surface temperature, *J. Clim.* 20 5473–96

863 Ruthrof, K. X., Breshears, D. D., Fontaine, J. B., Froend, R. H., Matusick, G., Kala, J., Miller,
864 B. P., Mitchell, P. J., Wilson, S. K., van Keulen, M., Enright, N. J., Law, D. J., Wernberg, T.,
865 & Hardy, G. E. S. J. (2018). Subcontinental heat wave triggers terrestrial and marine, multi-
866 taxa responses. *Scientific Reports*, 8(1), 1–9. <https://doi.org/10.1038/s41598-018-31236-5>



- 867 Savu, A. (2022). Temperature Highs, Climate Change Salience, and Eco-Anxiety: Early
868 Evidence from the 2022 United Kingdom Heatwave. *Climate Change Salience, and Eco-*
869 *Anxiety*
- 870 Sims, D. W., Wearmouth, V. J., Genner, M. J., Southward, A. J., & Hawkins, S. J. (2004).
871 Low-temperature-driven early spawning migration of a temperate marine fish. *Journal of*
872 *Animal Ecology*, 73(2), 333-341.
- 873 Smale, D. A., Wernberg, T., Oliver, E. C. J., Thomsen, M., Harvey, B. P., Straub, S. C.,
874 Burrows, M. T., Alexander, L. V., Benthuisen, J. A., Donat, M. G., Feng, M., Hobday, A. J.,
875 Holbrook, N. J., Perkins-Kirkpatrick, S. E., Scannell, H. A., Sen Gupta, A., Payne, B. L., &
876 Moore, P. J. (2019). Marine heatwaves threaten global biodiversity and the provision of
877 ecosystem services. *Nature Climate Change*, 9(4), 306–312. [https://doi.org/10.1038/s41558-](https://doi.org/10.1038/s41558-019-0412-1)
878 [019-0412-1](https://doi.org/10.1038/s41558-019-0412-1)
- 879 Seuront, L., Nicastro, K. R., Zardi, G. I., & Goberville, E. (2019). Decreased thermal
880 tolerance under recurrent heat stress conditions explains summer mass mortality of the blue
881 mussel *Mytilus edulis*. *Scientific Reports*, 9(1), 1–14. [https://doi.org/10.1038/s41598-019-](https://doi.org/10.1038/s41598-019-53580-w)
882 [53580-w](https://doi.org/10.1038/s41598-019-53580-w)
- 883 Schlegel R.W., E.C.J. Oliver, T. Wernberg, A.J. Smit (2017) Nearshore and offshore co-
884 occurrence of marine heatwaves and cold-spells, *Progress in Oceanography*, 151, 189-205.
885 <https://doi.org/10.1016/j.pocean.2017.01.004>
- 886 Schlegel, R. W., Darmaraki, S., Benthuisen, J. A., Filbee-Dexter, K., Oliver, E. C. J. (2021)
887 Marine cold-spells, *Progress in Oceanography*, 198, 102684.
888 <https://doi.org/10.1016/j.pocean.2021.102684>
- 889 Simon, A., Plecha, S. M., Russo, A., Teles-Machado, A., Donat, M. G., Auger, P. A., &
890 Trigo, R. M. (2022). Hot and cold marine extreme events in the Mediterranean over the period
891 1982-2021. *Frontiers in Marine Science*, 9(August), 1–12.
892 <https://doi.org/10.3389/fmars.2022.892201>
- 893 Southward, A. J. (1960). On changes of sea temperature in the english channel. *Journal of the*
894 *Marine Biological Association of the United Kingdom*, 39(3), 449–458.
895 <https://doi.org/10.1017/S0025315400013473>
- 896 Wang, Y., Kajtar, J. B., Alexander, L. V., Pilo, G. S., & Holbrook, N. J. (2022).
897 Understanding the changing nature of marine cold-spells. *Geophysical Research Letters*, 49,
898 e2021GL097002. <https://doi.org/10.1029/2021GL097002>
- 899 Wethey, D. S., & Woodin, S. A. (2022). Climate change and *Arenicola marina*: Heat waves
900 and the southern limit of an ecosystem engineer. *Estuarine, Coastal and Shelf Science*,
901 276(December 2021), 108015. <https://doi.org/10.1016/j.ecss.2022.108015>



25

902 Wernberg, T., Bennett, S., Babcock, R. C., De Bettignies, T., Cure, K., Depczynski, M.,
903 Dufois, F., Fromont, J., Fulton, C. J., Hovey, R. K., Harvey, E. S., Holmes, T. H., Kendrick,
904 G. A., Radford, B., Santana-Garcon, J., Saunders, B. J., Smale, D. A., Thomsen, M. S.,
905 Tuckett, C. A., Tuya, F., Vanderklift, M. A., & Wilson, S. (2016). Climate-driven regime shift
906 of a temperate marine ecosystem. *Science*, 353(6295), 169–172.
907 <https://doi.org/10.1126/science.aad8745>
908
909 Vogel, M. M., Zscheischler, J., Wartenburger, R., Dee, D., & Seneviratne, S. I. (2019).
910 Concurrent 2018 hot extremes across Northern Hemisphere due to human-induced climate
911 change. *Earth's future*, 7(7), 692-703. <https://doi.org/10.1029/2019EF001189>
912
913 Yao, Y., Wang, C., & Fu, Y. (2022). Global Marine Heatwaves and Cold-Spells in Present
914 Climate to Future Projections. *Earth's Future*, 10(11), e2022EF002787.
915
916 Yiou, P., Cattiaux, J., Faranda, D., Kadygrov, N., Jézéquel, A., Naveau, P., Ribes, A., Robin,
917 Y., Thao, S., Oldenborgh, G. J. & Vrac, M. (2020). Analyses of the Northern European
918 summer heatwave of 2018. *Bulletin of the American Meteorological Society*, 101(1), S35-S40.
919 <https://doi.org/10.1175/BAMS-D-19-0170.1ff>.
920
921
922
923
924
925
926
927
928
929
930
931
932
933
934
935
936
937
938
939
940
941
942
943
944